

Article

Highly Active Catalysts Based on the $\text{Rh}_4(\text{CO})_{12}$ Cluster Supported on $\text{Ce}_{0.5}\text{Zr}_{0.5}$ and Zr Oxides for Low-Temperature Methane Steam Reforming

Andrea Fasolini¹, Silvia Ruggieri¹, Cristina Femoni^{1,2} and Francesco Basile^{1,2,*}

¹ Department of Industrial Chemistry “Toso Montanari”, University of Bologna, V.le Risorgimento, 4, 40136 Bologna, Italy; andrea.fasolini2@unibo.it (A.F.); silvia.ruggieri3@unibo.it (S.R.); cristina.femoni@unibo.it (C.F.)

² Consorzio Interuniversitario Reattività e Catalisi (CIRCC), 70126 Bari, Italy

* Correspondence: f.basile@unibo.it; Tel.: +39-0512093663

Received: 8 August 2019; Accepted: 23 September 2019; Published: 25 September 2019



Abstract: Syngas and Hydrogen productions from methane are industrially carried out at high temperatures (900 °C). Nevertheless, low-temperature steam reforming can be an alternative for small-scale plants. In these conditions, the process can also be coupled with systems that increase the overall efficiency such as hydrogen purification with membranes, microreactors or enhanced reforming with CO₂ capture. However, at low temperature, in order to get conversion values close to the equilibrium ones, very active catalysts are needed. For this purpose, the $\text{Rh}_4(\text{CO})_{12}$ cluster was synthesized and deposited over $\text{Ce}_{0.5}\text{Zr}_{0.5}\text{O}_2$ and ZrO_2 supports, prepared by microemulsion, and tested in low-temperature steam methane reforming reactions under different conditions. The catalysts were active at 750 °C at low Rh loadings (0.05%) and outperformed an analogous Rh-impregnated catalyst. At higher Rh concentrations (0.6%), the Rh cluster deposited on $\text{Ce}_{0.5}\text{Zr}_{0.5}$ oxide reached conversions close to the equilibrium values and good stability over long reaction time, demonstrating that active phases derived from Rh carbonyl clusters can be used to catalyze steam reforming reactions. Conversely, the same catalyst suffered from a fast deactivation at 500 °C, likely related to the oxidation of the Rh phase due to the oxygen-mobility properties of Ce. Indeed, at 500 °C the Rh-based ZrO_2 -supported catalyst was able to provide stable results with higher conversions. The effects of different pretreatments were also investigated: at 500 °C, the catalysts subjected to thermal treatment, both under N_2 and H_2 , proved to be more active than those without the H_2 treatment. In general, this work highlights the possibility of using Rh carbonyl-cluster-derived supported catalysts in methane reforming reactions and, at low temperature, it showed deactivation phenomena related to the presence of reducible supports.

Keywords: Hydrogen; Low Temperature Steam Reforming; $\text{Rh}_4(\text{CO})_{12}$ cluster; microemulsion synthesis; CeZr oxide; Zr oxide

1. Introduction

Methane steam reforming (SR) is a leading reaction in syngas production with a wide employment on an industrial scale [1–6]. However, in order to allow high conversions of methane, very high temperatures (900 °C) are employed, and this requires feeding the reactor with a large amount of heat, which is provided by burning part of the methane reagent in an external furnace. Therefore, in some conditions, lower operative temperatures (400–500 °C) may be advisable, for instance when very high H_2/CO ratios are required, in what is called Low Temperature Steam Reforming (LTSR) [7–9]. In cases of excess of steam in the process feed, with the right catalyst the two SR and WGS (Water Gas Shift) reactions take place consequently in the same reactor [10,11]. This allows for a drastic decrease in CO

content with respect to the classical steam reforming reaction, providing an outlet gas with a high H_2/CO ratio. Moreover, the temperatures employed are compatible with special applications such as use of microreactors, CO_2 capture enhanced reforming, and Pd membrane reactors for pure hydrogen production [12–15]. In the latter case, the steam reforming occurs inside a tubular membrane from which hydrogen is separated. The employment of a membrane requires high operative pressures that reduce the methane conversion. However, the hydrogen removal from the retentate allows to increase the hydrogen yield and methane conversion with regard to a classical reactor, allowing to realize an effective process [11,12]. For these reasons, very active, selective, and stable catalysts are required to efficiently perform LTSR in a membrane reactor. In fact, these must be able to activate methane at low temperatures, thus improving the performances with respect to high active SR and CPO (catalytic partial oxidation) catalysts [16]. Moreover, active-phase stability is important for the application cited above, in order to minimize the operations related to catalyst replacement. For this reason, Rh was selected as active phase rather than the mostly used Ni. In fact, Rh was reported to have both higher activity and stability in steam reforming than other active phases [17–21].

The $Rh_4(CO)_{12}$ cluster [22] had been studied almost 30 years ago for catalyzing different reactions, such as the hydrosilylation of isoprene, cyclohexanone, and cyclohexenone [23], or, more recently, the hydroformylation of cyclopentene co-promoted by $HMn(CO)_5$ [24], all in homogeneous catalysis. $Rh_4(CO)_{12}$ -derived catalysts, supported on Al_2O_3 , MgO , and CeO_2 , had also been tested in 2001 in the CPO process for syngas production [25–27]. However, the CPO conditions and the related generated hot spot do not allow a simple comparison among catalysts. Furthermore, no tests on heterogeneous supported catalysts based on the $Rh_4(CO)_{12}$ cluster have been reported yet.

This work describes the preparation of Rh-based oxide-supported catalysts by exploiting the $Rh_4(CO)_{12}$ carbonyl cluster as source of active phase, as well as their performances on low-temperature methane steam reforming reactions, with the aim of developing a suitable catalyst for future membrane reactor operations. The $Rh_4(CO)_{12}$ cluster was deposited on two different supports, namely $Ce_{0.5}Zr_{0.5}O_2$ and ZrO_2 , which were obtained by microemulsion synthesis. Notably, this method gave rise to an improved Rh-supported CeZr-oxide catalyst with respect to classical CeZr ones, in terms of activity and stability in the oxy-reforming reaction [28–31].

The effect of the presence of Ce in the support and its influence on the catalyst deactivation were also investigated. Noteworthy, no deactivation studies of $Rh_4(CO)_{12}$ -derived catalysts for syngas production have been reported thus far.

2. Results

2.1. Preparation and Characterization of the Supported Catalysts

The CeZr and Zr oxide supports were synthesized by *w/o* microemulsion technique [28] followed by calcination at 750 °C, and were characterized by XRD (X-Ray Diffraction) analyses (Figure 1). The diffractogram of the former showed reflections ascribable to the $Ce_{0.5}Zr_{0.5}O_2$ (CZO) phase, which is not easy to obtain with other synthetic methods in terms of composition homogeneity and structure. This specific phase possesses higher oxygen mobility and storage properties that enhance the activity in reforming reactions [28]. Debye Scherrer calculations on the peak at lower 2θ showed an average crystallite dimension of 8 nm.

The XRD analysis on the zirconium oxide sample, ZrO_2 (ZO), showed the formation of the sole tetragonal phase of zirconia, while the pattern related to the monoclinic phase, associated with a lower surface area [32–35], was not present. Debye Scherrer calculations gave an average crystallite dimension of 10 nm.

Table 1 shows the surface area, volume of the pores, and average pore diameter of the CZO and ZO samples, determined through Barrett-Joyner-Helenda (BJH) analysis.

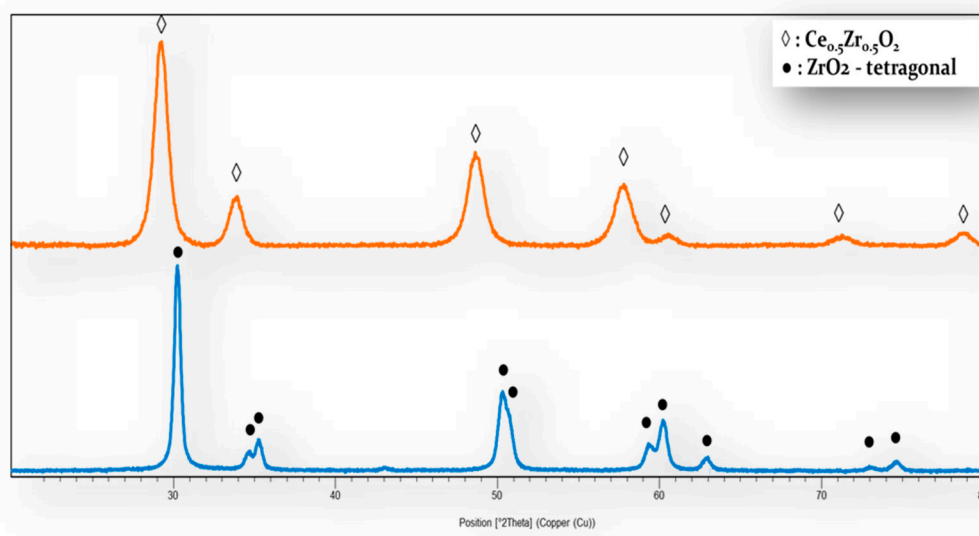


Figure 1. X-Ray Diffraction (XRD) spectra of the $\text{Ce}_{0.5}\text{Zr}_{0.5}\text{O}_2$ (CZOm) and ZrO_2 (ZOm) samples synthesized by microemulsion and followed by calcination at 750 °C.

Table 1. Surface area, pore volume, and average pore diameter of the CZOm and ZOm.

	Surface Area (m^2/g)	Pore Vol. (cm^3/g)	Avg. Pore Diam (nm)
CZOm	48.8	0.08	5.8
ZOm	40.7	0.07	10.8

The Ce-containing sample showed a higher surface area and a smaller average pore diameter. This is related to the smaller average particle dimension that was obtained for the Ce-containing sample (8 nm) compared to the zirconium oxide one. In any case, high surface and small particles were obtained thanks to the microemulsion technique, in which micelles, used as microreactors, helped to modulate the crystallite dimensions during the synthesis. Nevertheless, the total pore volume was similar for the two samples, suggesting that a higher number of smaller pores was found in the CZOm sample.

The two supports were also analyzed through IR (Infrared) spectroscopy in the solid state, in nujol mull between NaCl plates, both before and after the deposition with the $\text{Rh}_4(\text{CO})_{12}$ cluster, in order to verify that this actually occurred. Initially, both spectra showed peaks at ca. 2100 (w), 2031 (s) and 1892 (w) cm^{-1} , typically associated to the sole supports. The cluster compound was then deposited on CZOm and ZOm (Rh loading of 0.6% wt/wt). The preparation was carried out by mixing a n-hexane solution of $\text{Rh}_4(\text{CO})_{12}$ with a slurry of the desired support in the same solvent for 24 hours, under CO atmosphere because of the instability of the neutral cluster in air. In the end, the IR spectra of the n-hexane solutions showed a complete absence of any residual $\text{Rh}_4(\text{CO})_{12}$, as indicated by the disappearance of its typical νCO absorptions. Moreover, both supports changed their colors from white to light burgundy after the treatment with the cluster and their IR spectra showed significant changes with respect to the initial ones. More specifically, the spectrum recorded on CZOm exhibited νCO peaks at 2078 (sh), 2051 (s), 2043 (m), 2019 (sh), 1803 (sh) and 1797 (w) cm^{-1} , while the one of ZOm showed νCO peaks at 2068 (w), 2038 (s), 1990 (sh) and 1774 (w) cm^{-1} . These experimental evidences consistently indicate that the cluster deposition on the CZOm and ZOm supports occurred. Figures 2 and 3 show the solid-state IR spectra of the bare and Rh-deposited CZOm and ZOm supports, respectively.

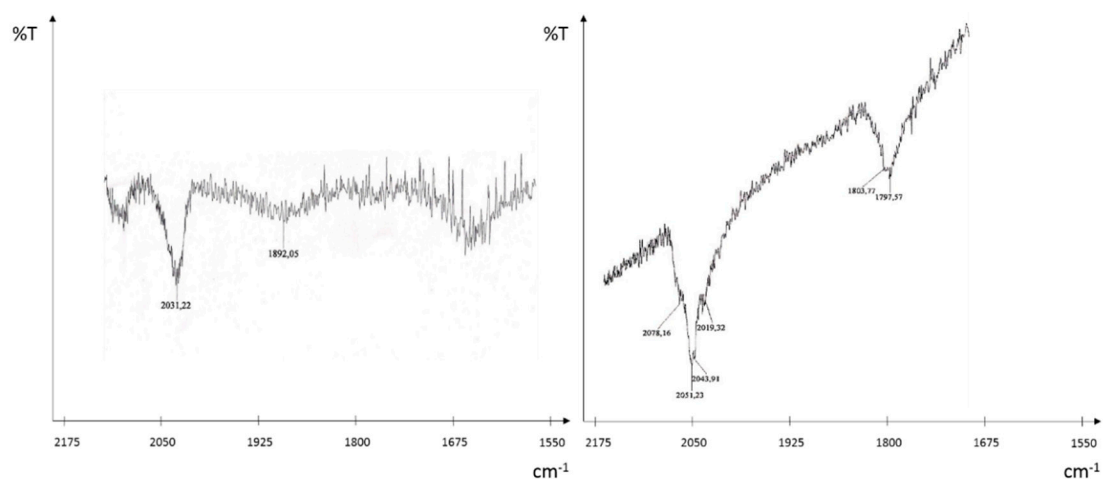


Figure 2. Solid-state infrared (IR) spectra of the bare (left) and Rh-deposited (right) CZOm support.

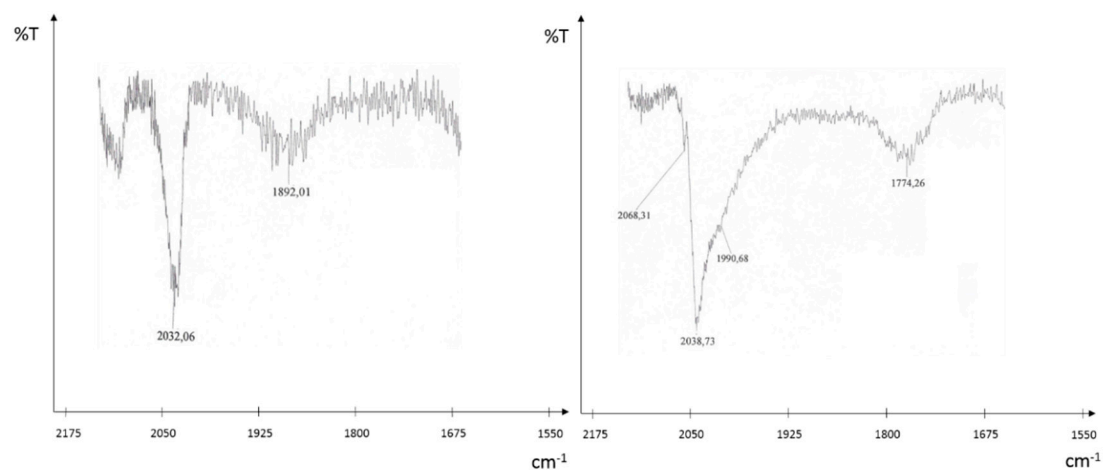


Figure 3. Solid-state IR spectra of the bare (left) and Rh-deposited (right) ZOm support.

Subsequently, both catalysts were pelleted and treated under N_2 at $500\text{ }^\circ\text{C}$, and new nujol mull spectra were recorded. As illustrated in Figure 4, the ZOm-supported catalyst exhibited residual νCO peaks at 2023 (w) and 1874 (w) cm^{-1} , while the CZOm-supported one displayed the same peaks shown by the support before the deposition [26].

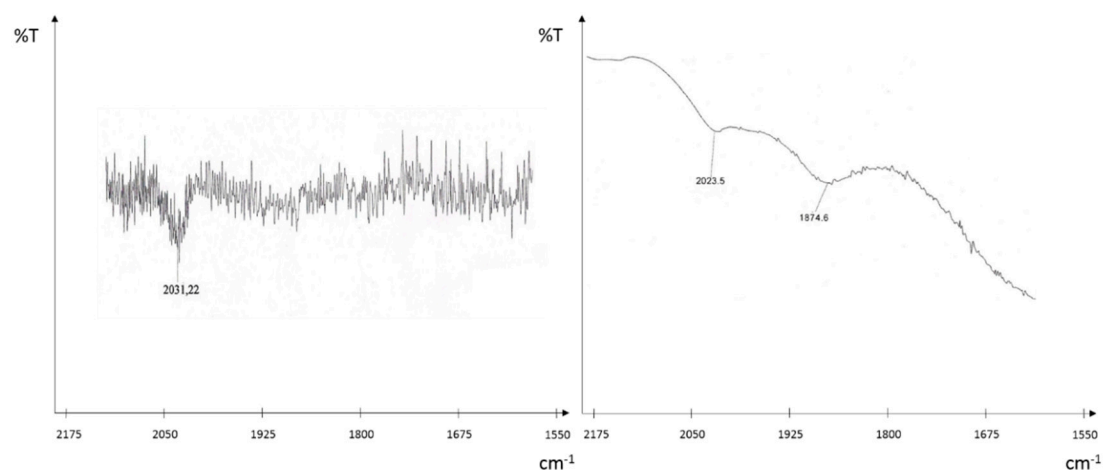


Figure 4. Solid-state IR spectra of the Rh-deposited CZOm (left) and ZOm (right) supports after treatment under N_2 at $500\text{ }^\circ\text{C}$.

A possible explanation for this different behavior could be that, in the CZOm support, the high mobility of oxygen atoms linked to the Ce(IV)/Ce(III) couple favored the complete oxidation of the Rh carbonyls [36]. After treatment under hydrogen flow at 500 °C, both catalysts only showed IR bands associated to the sole supports.

2.2. Catalytic Tests on Cluster-Derived Catalysts

2.2.1. Cluster-Based Catalyst with High Rh Loading

The cluster-based catalyst with a metal loading of 0.6% deposited on Ce_{0.5}Zr_{0.5}O₂ (Rh0.6-CL-R-CZOm) was tested in different conditions, and the effects of the S/C (Steam/Carbon) ratio, temperature, pressure and GHSV (Gas Hourly Space Velocity) were studied. The precursor was charged in the reactor and heated under N₂ at 500 °C, and after cooling down to 200 °C, the sample was heated at 500 °C under H₂ to obtain the final active catalyst. The analyses of the reaction parameters have been carried out with the aim of studying the conditions with which the catalyst could maximize both syngas and hydrogen productions.

At 500 °C, the increase of the S/C ratio had a positive effect on the methane conversion (X_{CH_4}), as shown in Figure 5. In particular, at low S/C ratios, the methane conversion was 19% at S/C 1 and 22% at S/C 1.5, very close to the equilibrium values (19% and 24%, respectively). A further increase in S/C up to 2 and 3 resulted in higher conversions of 23% and 26%, though not enough to meet the increase of the equilibrium values (29% and 36%, respectively), deriving from higher steam concentration, showing a kinetic limitation of the steam reforming reaction. The H₂/CO ratio was also considered to analyze the contribution of the water gas shift reaction (WGSR). In all conditions, the ratio was higher than the stoichiometric value of 3, due to the occurrence of the WGSR. Thus, an advantage of low temperature steam reforming is the possibility of carrying out the two reactions together, as opposed of conducting them in three different reactors (one for steam reforming, a high-temperature shift reactor and a low-temperature shift one), which is the usual procedure. For instance, a H₂/CO ratio of 28 was obtained at S/C 1. When the S/C ratio increased, the H₂/CO raised thanks to an augmented contribution of the WGSR, reaching the values of 35, 43, and 63 at S/C 1.5, 2 and 3, respectively. Indeed, the high amount of steam reacted with CO and produced a major amount of hydrogen. This was also confirmed by the CO selectivity (s_{CO}), which decreased when increasing S/C, falling from 13 (at S/C 1) down to 6 at S/C 3.

Figure 6 highlights the effect of the temperature on the catalytic conversion of methane at 30,000 h⁻¹, S/C 3 and atmospheric pressure. In all conditions, the methane conversions were far from the equilibrium values (indicated by the empty bars). In general, experimental and equilibrium methane conversions increase with temperature as both steam reforming thermodynamics and kinetics are favored at high temperature. In fact, a conversion of 4% was observed at 350 °C, far from the equilibrium value of 11%, which increased to 9% and 17% at 400 and 450 °C, but they were both still far from the equilibrium conversions (18% and 26%, respectively). The equilibrium value was not reached even at 500 °C, where the observed experimental conversion was 26% and the equilibrium one 36%. However, a sharply decreasing trend was observed for the H₂/CO ratio. The WGS and SR reactions are favored in opposite conditions; therefore, at 350 °C water gas shift was predominant, and the as-produced CO was directly converted into hydrogen, resulting in a final gas composition with CO concentration of 75 ppm. Conversely, at 500 °C the water gas shift is less favored, and an increased rate of steam reforming consumed water, further depressing the WGSR. Overall, this resulted in a decrease of the H₂/CO ratio from 1700 at 350 °C to 63 at 500 °C, and in an increase of the CO selectivity with temperature up to 6%.

An increase of the GHSV caused a decrease in the methane conversion from 23% at 30,000 h⁻¹, to 17% at 50,000 h⁻¹ and 13% at 100,000 h⁻¹, which also resulted in lower hydrogen production (Figure 7). Moreover, the conversion values were far from the equilibrium ones, which were set at 29%, 28%, and 25%, respectively. This was due to the minor contact time between the gas stream and the

catalyst. In these conditions, in fact, the reaction appeared to be strongly limited by kinetics, and the catalyst gave conversion results that were far from the thermodynamic equilibrium. The lower methane conversion is accompanied by a higher water partial pressure, which decreased the CO amount due to WGS and, overall, increased the H_2/CO ratio from 43 at $30,000\text{ h}^{-1}$, to 66 at $50,000\text{ h}^{-1}$ and 91 at $100,000\text{ h}^{-1}$. This catalyst behavior showed the predominance of the WGS in determining the H_2/CO ratio, suggesting a faster kinetics for the WGS reaction over the steam reforming one. However, it is difficult to offer a complete comparison among the different tests as lower catalytic bed temperatures are developed at higher GHSV, due to decreased conversions. In fact, lower temperatures decrease the equilibrium conversion and steam reforming activities.

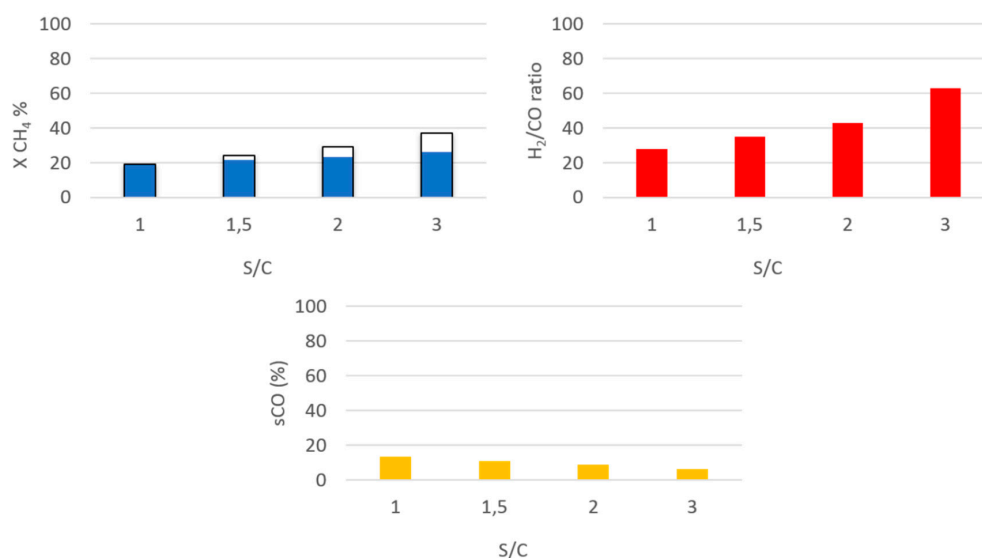


Figure 5. Comparison among tests carried out on Rh0.6-CL-R-CZOm at $30,000\text{ h}^{-1}$, 1 atm and $500\text{ }^\circ\text{C}$. The graphs report the methane conversion (blue) with respect to the equilibrium values (white bars with black frames), H_2/CO ratio (red), and CO selectivity (yellow) versus different S/C ratios.

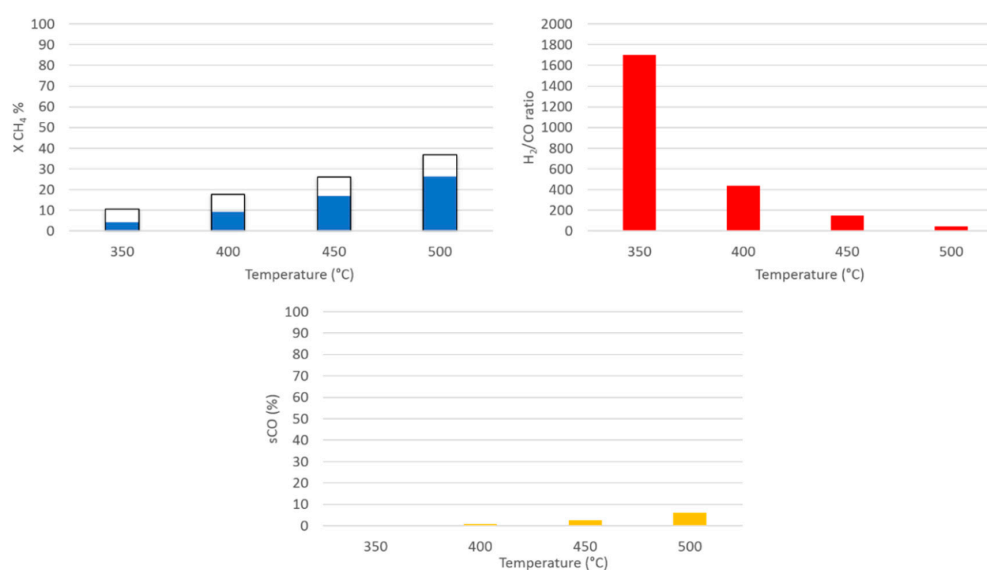


Figure 6. Comparison among tests carried out on Rh0.6-CL-R-CZOm at $30,000\text{ h}^{-1}$, 1 atm and S/C 3. The graphs report the methane conversion (blue) with respect to the equilibrium values (white bars with black frames), H_2/CO ratio (red), and CO selectivity (yellow) versus different T. The Y scale related to the H_2/CO -ratio graph is very different from the others due to the large values.

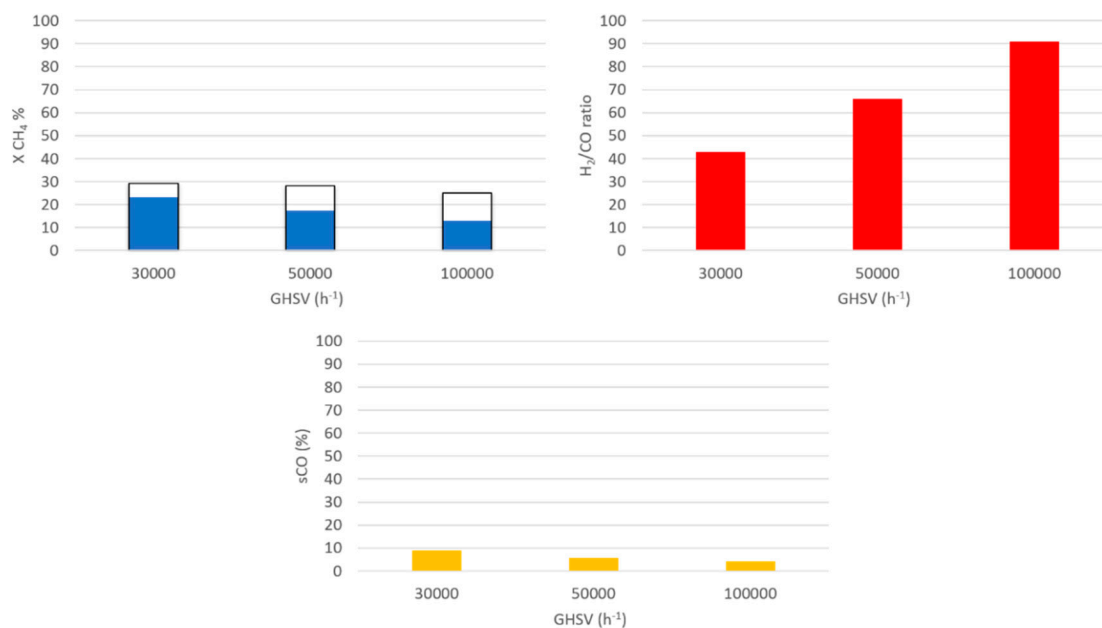


Figure 7. Comparison among tests carried out on Rh0.6-CL-R-CZOm at 1 atm, S/C 2 and 500 °C. The graphs report the methane conversion (blue) with respect to the equilibrium values (white bars with black frames), H₂/CO ratio (red) and CO selectivity (yellow) versus different Gas Hourly Space Velocity (GHSV).

At higher pressure, lower methane conversions were observed (from 29% at 1 atm, to 20%, 17%, and 13% at 3, 5, and 10 atm, respectively) (Figure 8), owing to a decreased thermodynamic equilibrium of the SR reaction. However, the equilibrium conversion was close to the experimental conversion at 5 atm (17%) and reached it at 10 atm (13%). In analogy with what observed above, a lower methane conversion is associated with a higher residual amount of water, which enhances the WGSR and, in turn, the H₂/CO ratio, which raised from 43 at 1 atm to 108 at 10 atm.

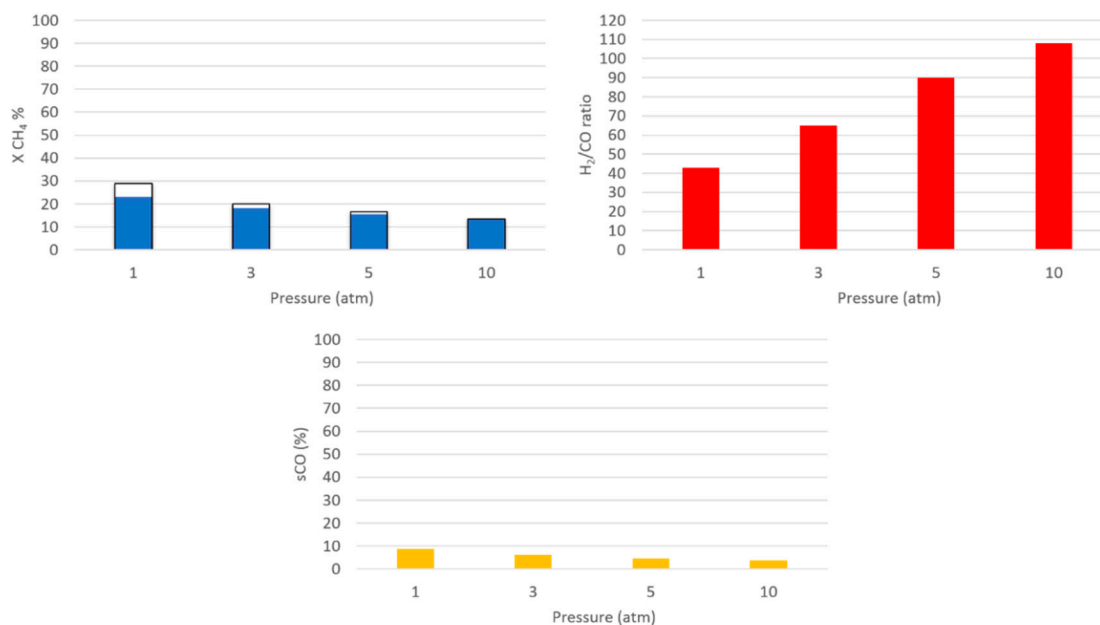


Figure 8. Comparison among tests carried out on Rh0.6-CL-R-CZOm at 30,000 h⁻¹, S/C 2 and 500 °C. The graphs report the methane conversion (blue) with respect to the equilibrium values (white bars with black frames), H₂/CO ratio (red) and CO selectivity (yellow) versus different GHSV. The Y scale related to the H₂/CO-ratio graph is slightly different from the others due to higher values.

The effect of the S/C ratio was investigated at 500 °C and 10 atm (Figure 9). In these conditions, the methane conversion increased with S/C, reaching the equilibrium values up to S/C 2 (9% at S/C 1, 11% at S/C 1.5 and 13% at S/C 2), and the experimental conversion (15%) close to equilibrium value (17%) at S/C 3. The highest conversion was observed at S/C 3 thanks to the increased equilibrium values at higher S/C ratios.

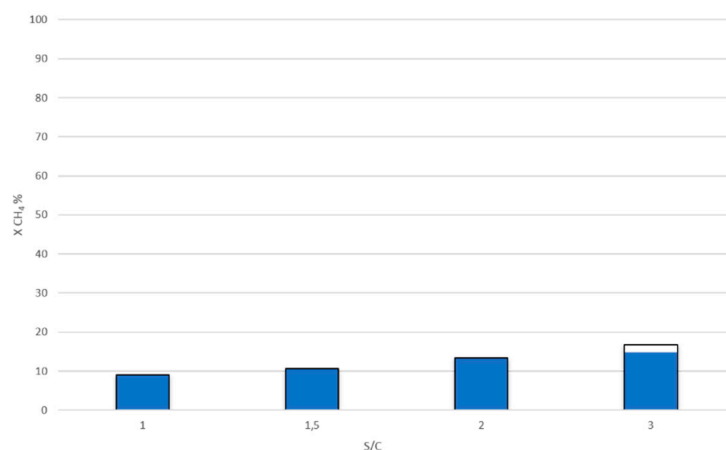


Figure 9. Comparison among tests carried out on Rh0.6-CL-R-CZOm at 30,000 h⁻¹, 10 atm and 500 °C. The graph reports the methane conversion (blue) with respect to the equilibrium values (empty bars with black frame) versus different S/C ratios.

The same tests were also conducted at lower temperature, namely 450 °C (Figure 10). In these operative conditions, the experimental methane conversion was close to the equilibrium values up to a S/C ratio of 2, however, it remained distant from it a S/C 3 due to the lower catalytic activity at this temperature. In particular, conversions of 5%, 6%, 7%, and 8% were, respectively, observed by increasing the S/C, while equilibrium conversions concurrently increased from 5% to 7%, then 9% and 12%.

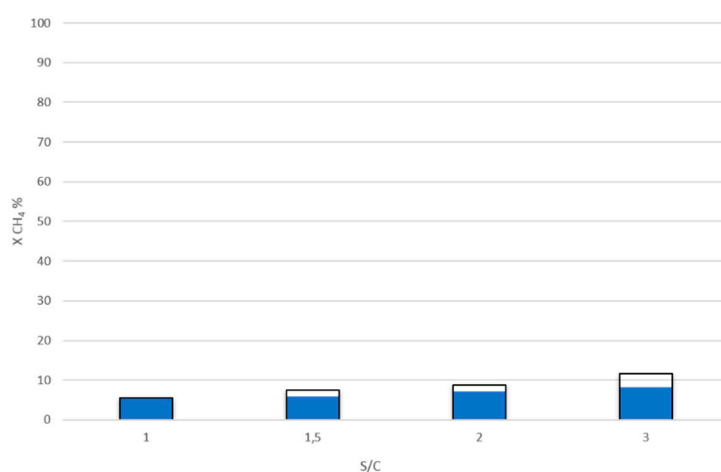


Figure 10. Comparison among tests carried out on Rh0.6-CL-R-CZOm at 30,000 h⁻¹, 10 atm and 450 °C. The graph reports the methane conversion (blue) with respect to the equilibrium values (empty bars with black frames) versus different S/C ratios.

Finally, in order to evaluate the stability of the catalysts in the operative conditions, a test with the same parameters as the first one (500 °C, 30,000 h⁻¹, 1 atm and S/C 1.5, Figure 11) was periodically conducted after every three tests carried out in different conditions, giving rise to the so-called return tests. The results indicate a rather high catalyst stability towards methane conversion. However,

a conversion drop of 4% was observed in the last return test, which was carried out after those conducted at low temperature and high pressure.

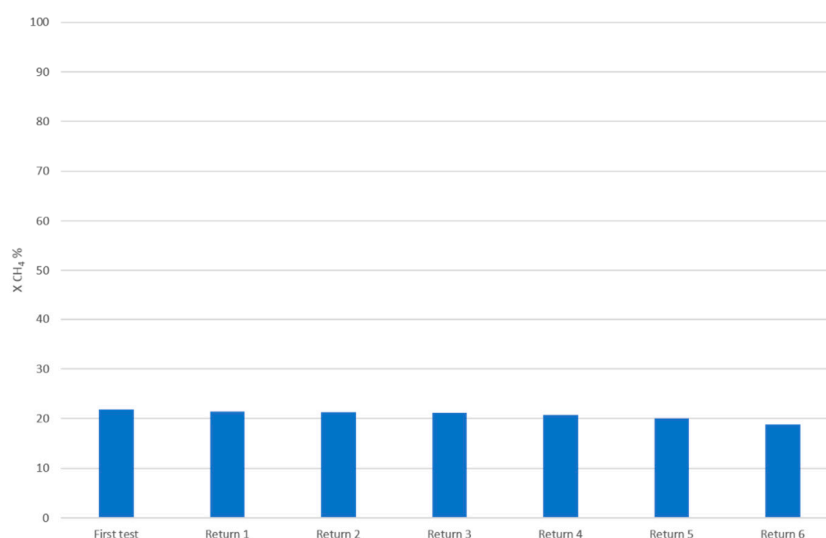


Figure 11. Methane conversion in deactivation tests carried out at 500 °C, 1 atm, 30,000 h⁻¹ and S/C 1.5.

This deactivation could be due to the formation of carbon on the active site, owing to Boudouard reaction, which in fact is favored at low temperature and high pressure. The Raman analysis on the spent Rh0.6-CL-R-CZOm catalyst (Figure 12) showed two very small peaks related to the presence of carbon. In particular, the bands detected at 1350 and 1580 cm⁻¹ could be attributed to the D-band and G-band of carbon, respectively [37–39]. In general, the G-band derives from the stretching of sp² carbon bonds in planes of graphene type [28], while the D-band is caused by the vibrations of carbon atoms in disordered species, such as amorphous carbon [40]. Both bands are rather broad and weak even after a long time on stream and different reaction test conditions, demonstrating the properties of the Ce_{0.5}Zr_{0.5}O₂ support synthesized by microemulsion in retarding carbon formation, which was also reported previously [28]. Considering the weakness of the bands, other phenomena, such as the re-oxidation of the catalyst during high-pressure tests, where high water partial pressure is present, need to be taken into account. In those conditions, especially in the first part of the catalytic bed where the presence of hydrogen is still very low, the gas mixture had a higher oxidative potential that could affect the oxidation state of the Rh.

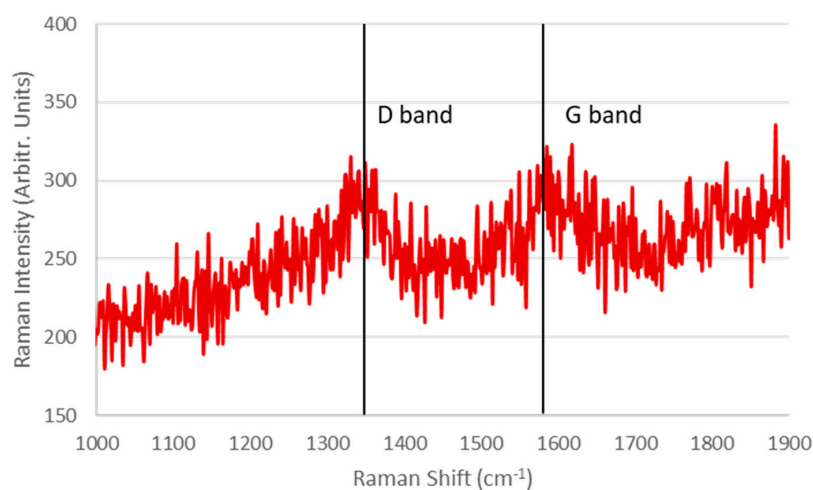


Figure 12. Raman analysis carried out on the used Rh0.6-CL-R-CZOm catalyst. The two bars indicate the presence of carbon.

2.2.2. Catalytic Tests with Low Rh Loading

The catalysts with a lower Rh loading were prepared diluting the 0.6% sample down to 0.05% wt/wt for further tests, to allow a better evaluation of the activity in a kinetic regime and a better understanding of the deactivation phenomena and metal support effects. Furthermore, the study of catalysts with low amounts of active phase is interesting for some specific applications, such as structured catalysts, membrane reactors, and microreactors, where the active phase may be deposited or coated in thin layers or on low-surface-area supports.

Catalysts with a low % of active phase (0.05% wt/wt) on the two different supports (CZOm and ZOm) were prepared and treated in two different ways: either just heated under N₂ or treated firstly under inert gas and then hydrogen. The four produced catalysts were named as follows:

- Rh0.05-CL-N-CZOm (the cluster-based catalyst deposited on CZOm was heated under nitrogen before the tests).
- Rh0.05-CL-R-CZOm (like the previous catalyst, also treated under H₂).
- Rh0.05-CL-N-ZOm (the cluster-based catalyst deposited on ZOm was heated under nitrogen before the tests).
- Rh0.05-CL-R-ZOm (like the previous catalyst, also treated under H₂).

Tests were carried out at fixed experimental conditions (GHSV = 30,000 h⁻¹, P = 1 atm, T = 500 °C, S/C 1.5) to compare the different catalysts' performances.

Before the catalytic tests, a preliminary screening was carried out to compare the Rh-particle size and distribution on the not-reduced (only heated under nitrogen) CZOm- and ZOm-supported catalysts. The TEM (Transmission Electron Microscopy) analyses performed on both supports evidenced the presence of small Rh particles (1-2 nm) with narrow size distribution (Figure 13). However, it is important to note that the identification of particles below 1 nm is difficult and may be strongly underestimated.

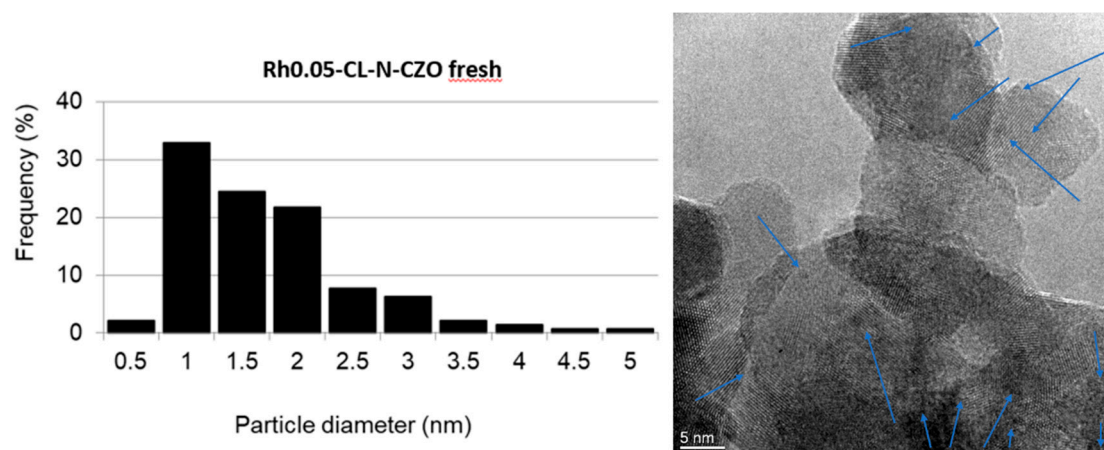


Figure 13. Rh particle-size distribution of the Rh cluster deposited on CZOm support determined by Transmission Electron Microscopy (TEM) analysis.

Figure 14 shows the results obtained with the cluster-based catalysts deposited on CZOm in tests carried out at high temperature. An initial conversion around 35% was observed for the catalyst not treated in hydrogen, with a decreasing trend in the first hour and an almost constant value of 30% during the reaction time. This result is in agreement with the fact that, when using such cluster-derived samples, active species are obtained even without the need of a reduction step (hydrogen treatment). The deactivation of the first part was probably due to the fast sintering of the reactive small particles evidenced by TEM analysis. The sample treated under H₂ was able to produce a higher conversion (40%) with stable results over 300 minutes.

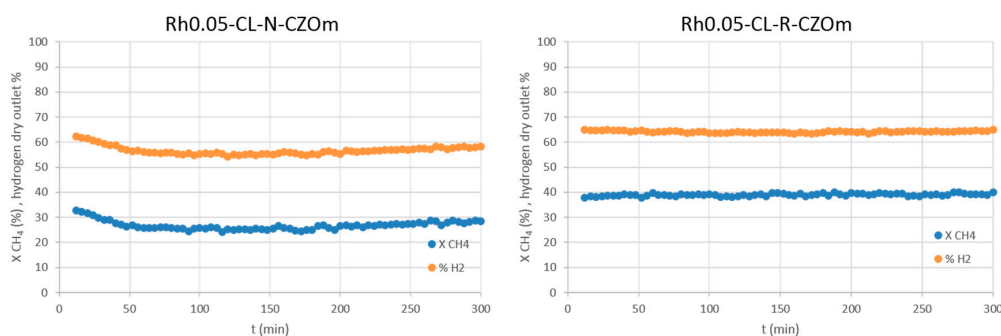


Figure 14. Methane conversion and hydrogen dry outlet percentage obtained on Rh0.05-CL-N-CZOm (left) and Rh0.05-CL-R-CZOm (right) tested at 750 °C, 30,000 h⁻¹, 1 atm and S/C 1.5.

The same test was conducted on an Rh-impregnated catalyst on the same CeZr oxide and reduced at 500 °C (Rh0.05-IWI-R-CZOm), which represents the best catalyst in oxy-reforming reaction [19] (Figure 15). This test showed an initial methane conversion of 36% with a slightly deactivation trend towards 34%. These results were lower than those obtained with Rh0.05-CL-R-CZO, indicating a higher activity for the cluster-derived catalyst and a readily stable conversion. This could be related to a better dispersion of the Rh cluster on the oxide support.

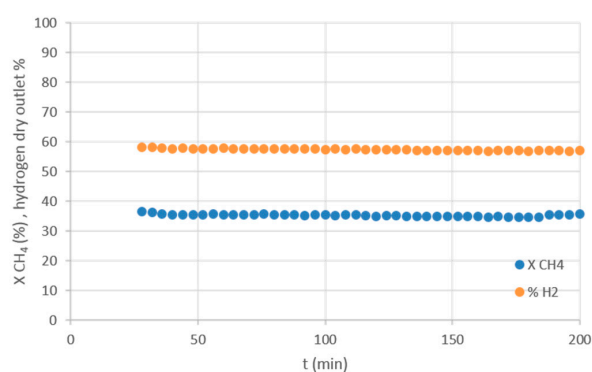


Figure 15. Methane conversion and hydrogen concentration in the dry gas obtained on Rh0.05-IWI-R-CZOm tested at 750 °C, 30,000 h⁻¹, 1 atm and S/C 1.5.

The same test was also conducted on the cluster-based catalyst supported on zirconia (Rh0.05-CL-R-ZOm, Figure 16) and treated under H₂, which gave a lower methane conversion (around 33%) with respect to the analogous cluster on CZOm. This is probably related to the effect of the Ce(IV)/Ce(III) couple in the sample that acts as steam-dissociating site, and by the higher oxygen mobility in the Ce_{0.5}Zr_{0.5}O₂ phase obtained with the microemulsion synthesis [28,41–44].

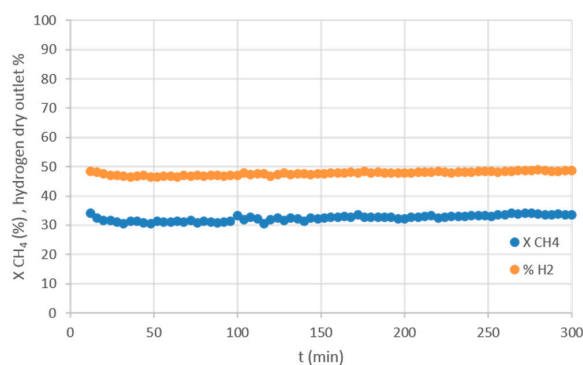


Figure 16. Methane conversion and hydrogen dry outlet percentage obtained on Rh0.05-CL-R-ZOm tested at 750 °C, 30,000 h⁻¹, 1 atm and S/C 1.5.

Having assessed the higher conversion of the cluster-based catalysts at 750 °C, the tests were also conducted at 500 °C. Figure 17 highlights the methane conversion and hydrogen dry outlet concentration versus the reaction time on the two CZOm-supported catalysts.

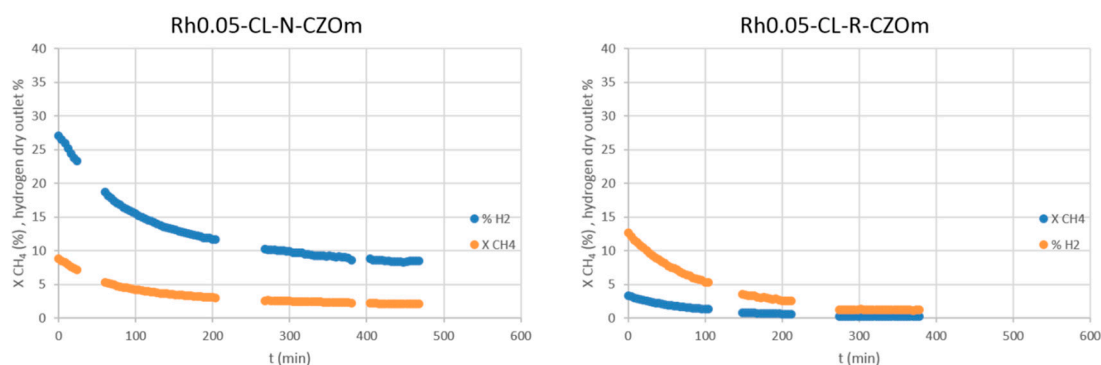


Figure 17. Methane conversion and hydrogen dry outlet percentage obtained on Rh0.05-CL-N-CZOm (left) and Rh0.05-CL-R-CZOm (right) tested at 500 °C, 30,000 h⁻¹, 1 atm and S/C 1.5.

The unreduced catalyst provided an initial conversion of circa 9%, while the reduced one gave an initial lower conversion (3%). It has been experimentally demonstrated that hydrogen treatment favors the formation of larger particles [26], and this phenomenon could explain the lower activity of the reduced catalyst with respect to the not-reduced one.

In order to explain the deactivation phenomena that took place in both catalysts, it is important to consider that the reaction environment at low temperature is an oxidizing one due to: i) the low amount of produced hydrogen related to lower kinetics of the catalyst, and also related to the low amount of active phase; ii) the high concentration of water. All this could favor the oxidation of Rh, which is faster when small particles are present, i.e., in the unreduced sample. The oxidation is very likely favored by the presence of Ce(IV) and the high oxygen mobility. The possibility to ascribe the deactivation to sintering of the active phase during reaction can be excluded, since small Rh particles were still found on the unreduced spent catalyst, as evidenced by TEM, where it is clear that the Rh metal particles are only slightly larger (centered between 1.5 and 2.5 nm, Figure 18) than those found on the fresh catalyst.

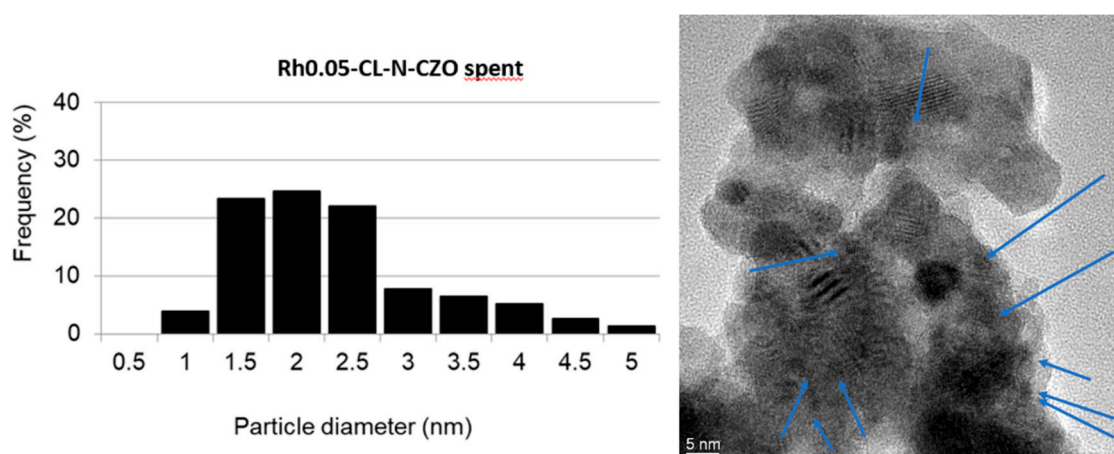


Figure 18. Particle size distribution of the spent Rh0.05-CL-N-CZOm determined via TEM analysis.

The catalytic performances of the Rh cluster deposited on ZOm, both not reduced and reduced (Rh0.05-CL-N-ZOm and Rh0.05-CL-R-ZOm), are shown in Figure 19.

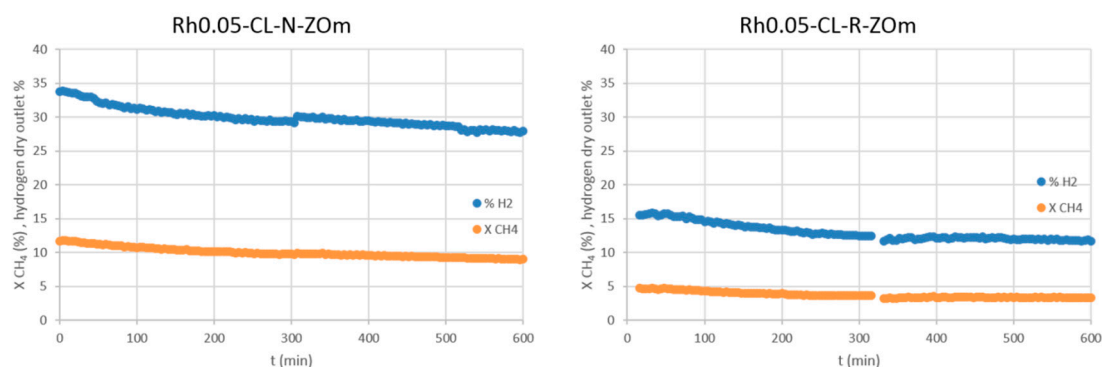


Figure 19. Methane conversion and hydrogen dry outlet percentage obtained on Rh0.05-CL-N-ZOm (left) and Rh0.05-CL-R-ZOm (right).

The initial conversion of the not-reduced catalyst (10.2%) was higher than the one reached with the CZOm-deposited cluster. Moreover, the fast deactivation that characterized the CZOm-based catalysts was not observed in this case, indicating that the presence of Ce favors the oxidation of the Rh. The reduced catalyst was stable too, but produced a lower conversion than the unreduced one, owing to the larger particles formed during the reduction step [26].

Table 2 reports the turnover frequency (TOF) values of the investigated catalysts at 500 °C. In the case of the CZOm samples, they were calculated on the initial conversion as those catalysts showed deactivation. Their comparison with TOF values of some other Rh-containing catalysts reported in the literature [45–47], however, is not always suggestive, because of the different supports, active-phase loadings, and operative conditions of the latter.

Table 2. Turnover frequency of the catalysts investigated in this work. * Calculated on the initial conversion.

Catalyst	T (°C)	S/C	GHSV (h ⁻¹)	P (atm)	TOF [molCH ₄ /(molRh*s)]
Rh0.05-CL-N-ZOm	500	1.5	30,000	1	1.47
Rh0.05-CL-R-ZOm	500	1.5	30,000	1	0.70
Rh0.05-CL-N-CZOm	500	1.5	30,000	1	1.32*
Rh0.05-CL-R-CZOm	500	1.5	30,000	1	0.73*

2.2.3. Investigation on Deactivation

It is particularly interesting to elucidate the mechanism of catalyst deactivation, since no such investigation on carbonyl cluster-derived catalyst is reported in literature, as very few low-temperature studies have been carried out. Having observed that the deactivation was related to the presence of Ce and the oxidizing environment, its cause was further investigated by TEM and EDS (Energy Dispersive X-ray Spectrometry) analyses. Having also excluded deactivation by sintering, and assessed the absence of carbon formed over the surface, it was hypothesized that the deactivation was caused by the oxidation of the active particles favored by Ce, which is able to provide oxygen to the active phase thanks to its redox properties, enhanced by the oxygen mobility of the microemulsion catalyst [19].

This phenomenon benefits from the oxidizing environment found in the low-temperature SR conditions, in which a relatively low amount of hydrogen is produced together with high concentrations of unreacted steam. SAED (Selected Area Electron Diffraction) analyses were carried out during TEM on the Rh particles of the unreduced CZOm- and ZOm-supported catalysts, after reaction at low (500 °C) and high (750 °C) temperature with the same Rh loading (0.05% wt/wt). In all samples, the presence of Rh in the analyzed particles was evidenced by the EDS analyses. The spent ZOm-supported samples, both at 500 °C and 750 °C, showed the presence of metallic Rh, as well as the CZOm-supported catalyst after reaction at high temperature (Figure 20). Experimental d-values of 2.25 and 1.84 Å, in fact, could be attributed to the metallic Rh phase, while those at 3.10 and 2.61 Å are related to the support.

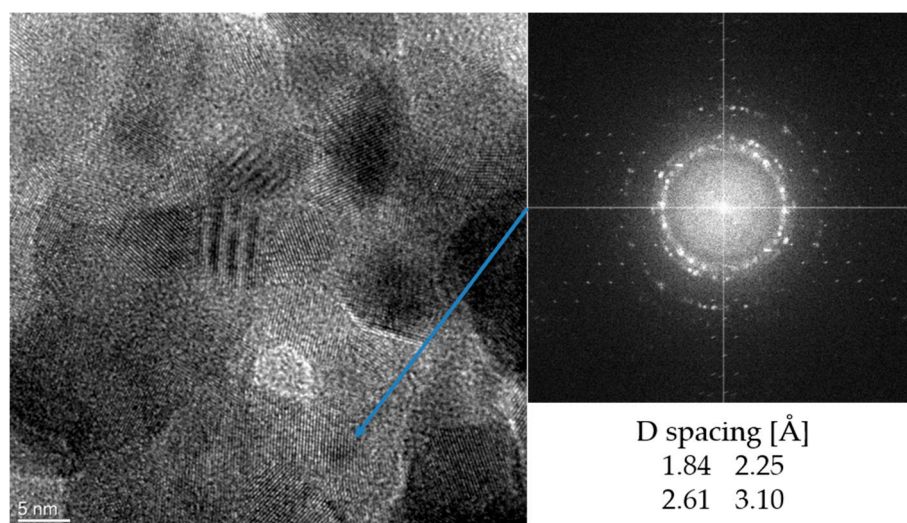


Figure 20. Selected Area Electron Diffraction (SAED) and TEM analyses carried out on a Rh containing area of the spent not-reduced CZOm supported catalyst after reaction at high temperature.

However, no such phase was observed in the spent CZOm-supported catalyst after reaction at low temperature (Figure 21); the measured d-values of 2.65 and 3.05 Å were attributed to the tetragonal phase of $\text{Ce}_{0.5}\text{Zr}_{0.5}\text{O}_2$. It was not possible to detect the presence of Rh oxide because its reflexes overlapped those of the support. Nonetheless, all these evidences can be confidently seen as an indirect confirmation that oxidation of Rh only occurred on the CZOm-supported catalyst after reaction at low temperature, which is the only one that showed deactivation.

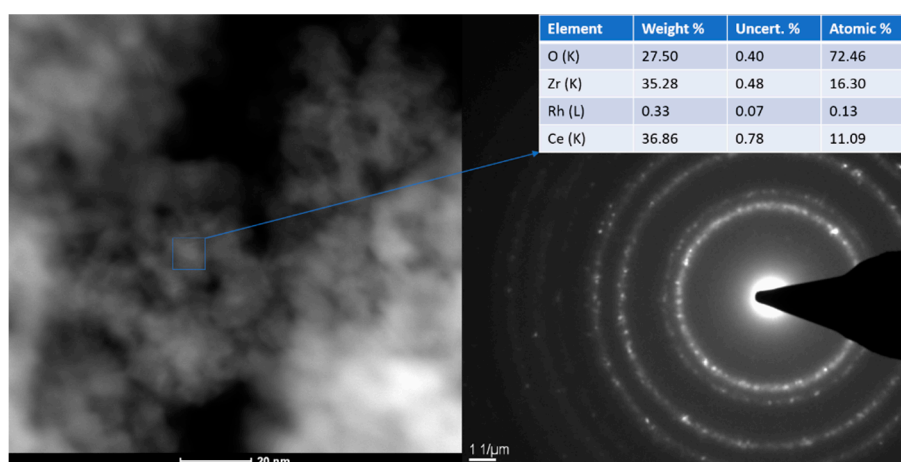


Figure 21. SAED and Energy Dispersive X-ray Spectrometry (EDS) analyses carried out on a Rh containing area of the spent not-reduced CZOm supported catalyst after reaction at low temperature.

The hypothesis of the oxidation of Rh is also substantiated by a computational study on metallic Rh clusters on CeO_2 , which showed that they are stable in reducing conditions such as those obtained in the high temperature steam reforming, but that the relative oxide is formed in oxidizing ones [36].

3. Materials and Methods

3.1. Catalysts Synthesis

Two supports, namely $\text{Ce}_{0.5}\text{Zr}_{0.5}\text{O}_2$ (CZOm) and ZrO_2 (ZOm), were prepared by *w/o* microemulsion technique as described elsewhere [28] and were calcined at 750 °C for 5 h with a heating ramp of

2 °C/min. In the case of ZrO₂ support, the microemulsion was heated to 70 °C for 30 min at the end of the synthesis in order to destroy the micelles.

The catalysts were prepared by reactive deposition of the Rh₄(CO)₁₂ cluster over the selected supports, namely CZOm and ZOm. In a typical experiment, the required amount of carbonyl cluster (0.6% of atomic Rh wt/wt of support) was dissolved in degassed n-hexane (10 mL) and added dropwise to a degassed n-hexane slurry of the desired support kept under CO atmosphere; the obtained slurry was then stirred for 24 h. The completion of the synthesis was evidenced by the discoloration of the solution and its IR analysis, which showed no peaks related to Rh₄(CO)₁₂ (ν CO at 2075 (vs), 2069 (vs) 2044 (m) and 1885 (s) cm⁻¹ in n-hexane). The solvent was thus removed in vacuum at room temperature. The catalyst was then stored under CO atmosphere and removed only to be pelletized and charged in the reactor, then readily kept under nitrogen flow and heated up to 500 °C. In order to provide a catalyst with a lower amount of Rh, the sample was diluted with bare CZOm or ZOm by 12 times, obtaining a catalyst with a loading of Rh of 0.05% (wt/wt of catalyst). In the case of reduced catalysts, the temperature was lowered to 200 °C then hydrogen (10% in nitrogen) was fluxed over the catalysts, while the temperature was again increased to 500 °C. After 15 h the hydrogen flux was stopped, and reactivity tests were carried out.

3.2. Catalyst Characterization

X ray diffraction analyses were carried out using a PW1050/81 diffractometer (Philips/Malvern, Royston, UK) equipped with a graphite monochromator in the diffracted beam and controlled by a PW1710 unit (Cu K α , λ = 0.15418 nm). A 2 θ range from 20° to 80° was investigated at a scanning speed of 40°/h. Nitrogen adsorption-desorption isotherms were determined at liquid nitrogen temperature (-196 °C), using an automatic ASAP 2020 absorptiometer (Micromeritics, Norcross, GA, USA) and analyzed using a software operating standard Brunauer–Emmett–Teller (BET) and BJH methods. Raman analysis was carried out with a micro-spectrometer Raman RM1000 (Renishaw/Thermo Fisher, New Mills, Wotton-under-Edge, Gloucestershire, UK) interfaced to a microscope Leica DMLM (objective 5 \times , 20 \times , 50 \times). The available sources were an Ar⁺ laser (λ = 514.5 nm; Pout = 25 mW) and a diode laser (λ = 780.0 nm; Pout = 30mW). In order to eliminate the Rayleigh scattering, the system was equipped with a notch filter for the Ar⁺ laser and an edge filter for the diode one. The network was a monochromator with a pass of 1200 lines/mm. The detector was a CCD one (Charge-Coupled Device) with a thermo-electrical cooling (203 K). TEM analyses were carried out using a TEM/STEM TECNAI F20 microscope (FEI, Hillsboro, OR, USA) combined with Energy Dispersive X-Ray Spectrometry (EDS), at 200 keV. The sample preparation was carried out by suspending the powder in ethanol and treating it with ultrasound for 15 min. The suspension was deposited on a “multifoil-carbon film” sustained by a Cu grid. Then the so-prepared system was dried at 100 °C.

3.3. Catalytic Tests

The catalysts were tested in a tubular INCOLOY800HT reactor (Meccanica Padana, San Nicolò (PI), Italy) (length 500 mm; internal diameter 10 mm) placed in a furnace as reported elsewhere [28,48]. The bed temperature was controlled with a thermocouple. 1.0 g of catalyst (30–60 mesh) was loaded into the reactor where the pretreatment and eventual reduction of the active phase were conducted by fluxing a 500 mL flow of N₂ or of an H₂/N₂ (10:90 v/v) gas mixture at 500 °C. Deionized water was fed by a HPLC pump (JASCO, Easton, MD, USA) and vaporized. The outlet gas (H₂, CO, CO₂, non-converted CH₄ and vapor) was condensed in order to eliminate water. The dry gas mixture was analyzed by a 490 micro gas chromatograph (Agilent Technologies, Cernusco sul Naviglio (MI), Italy) with two different columns. Hydrogen was separated through a MS5A 20 m long (carrier: N₂), while CH₄, CO, and CO₂ were separated with a CO_x column 1 m long (carrier: He). Both modules were equipped with a Thermal Conductivity Detector TCD. The CEA-NASA software was used to calculate the outlet composition of the stream at the thermodynamic equilibrium. The software gave the molar gaseous outlet composition (non-converted CH₄, non-converted H₂O, CO, CO₂, H₂, and deposited

carbon if present), based on the feed composition in terms of molar percentage, reaction temperature, and pressure. Methane conversion was taken as reference in order to evaluate the catalytic activities of the tested samples and was compared with the one calculated at the thermodynamic equilibrium. Methane conversion accuracy was evaluated by calculating standard deviation. This resulted to be lower than $\pm 0.9\%$ for the tests at $750\text{ }^{\circ}\text{C}$ and lower than $\pm 0.7\%$ in the tests at $500\text{ }^{\circ}\text{C}$; in a conservative way, we considered accuracy to be $\pm 1\%$ for the test at high temperature and $\pm 0.8\%$ for those at low temperature.

4. Conclusions

This paper describes the synthesis, characterization and catalytic behavior of Rh-based catalysts, obtained by using the $\text{Rh}_4(\text{CO})_{12}$ neutral cluster as the active-phase precursor. In particular, the preparation method allowed the deposition of the cluster on the surface of $\text{Ce}_{0.5}\text{Zr}_{0.5}\text{O}_2$ and ZrO_2 supports, which were synthesized by w/o microemulsion technique. The catalysts were found to be active in the low-temperature steam reforming process for syngas production. At high Rh loadings (0.6%) the CZOM-supported catalyst was active at $350\text{ }^{\circ}\text{C}$ and was able to reach the equilibrium conversion, especially at low S/C ratio or at high pressures at 450 and $500\text{ }^{\circ}\text{C}$. It showed good stability, and this opens the possibility of employing such catalyst in membrane reactors, enhanced reformers or chemical loop based on reforming. At lower concentrations (0.05%) and high temperature, the CZOM-supported cluster sample showed better results with respect to the analogous ZOM-supported one and to a classical Rh-impregnated CeZr catalyst. At low temperature, a deactivation effect was observed for the CZOM-supported catalyst, which could be overcome by employing a ZOM support. A detailed analysis provided evidences that the oxidation of the Rh promoted by Ce and high oxygen mobility was responsible for the fast deactivation. In these conditions, it was also observed that the cluster-based catalyst which had not been treated with hydrogen at $500\text{ }^{\circ}\text{C}$ was more active than the treated one, due to the sintering of the Rh particles. Finally, the unreduced 0.05% Rh cluster deposited on the ZrO_2 support showed significant activity at $500\text{ }^{\circ}\text{C}$.

Author Contributions: A.F. investigated the catalytic activity and the support characterization and wrote the first draft; S.R. investigated the cluster preparation and deposition, and collaborated to write the first draft; C.F. supervised the catalyst preparation, investigated the IR and cluster analysis, and collaborated in writing, reviewing, and editing; F.B. defined the methodology for support preparation, supervised the project, validated the catalytic data, and took care of the conceptualization and of writing, reviewing, and editing of the paper.

Funding: This research received no external funding.

Acknowledgments: The contribution of Francesca Ospitali of the Department of Industrial Chemistry “Toso Montanari” is acknowledged for the TEM analysis.

Conflicts of Interest: The authors declare no conflict of interest.

References

1. Rostrup-Nielsen, J.R. Catalytic Steam Reforming. In *Catalysis: Science and Technology*; Anderson, J.R., Boudart, M., Eds.; Catalysis; Springer: Berlin/Heidelberg, Germany, 1984; Volume 5, pp. 1–117. ISBN 978-3-642-93247-2.
2. Rostrup-Nielsen, J.R.; Christiansen, L.J.; Bak Hansen, J.-H. Activity of steam reforming catalysts: Role and assessment. *Appl. Catal.* **1988**, *43*, 287–303. [[CrossRef](#)]
3. Trimm, D.L. The Steam Reforming of Natural Gas: Problems and Some Solutions. In *Studies in Surface Science and Catalysis*; Bibby, D.M., Chang, C.D., Howe, R.F., Yurchak, S., Eds.; Methane Conversion; Elsevier: Amsterdam, The Netherlands, 1988; Volume 36, pp. 39–50.
4. El-Temtamy, S.A.; El-Salamony, R.A.; Ghoneim, S.A. Review on Innovative Catalytic Reforming of Natural Gas to Syngas. *World J. Eng. Technol.* **2016**, *4*, 720–726.
5. Taji, M.; Farsi, M.; Keshavarz, P. Real time optimization of steam reforming of methane in an industrial hydrogen plant. *Int. J. Hydrog. Energy* **2018**, *43*, 13110–13121. [[CrossRef](#)]

6. Azancot, L.; Bobadilla, L.F.; Santos, J.L.; Córdoba, J.M.; Centeno, M.A.; Odriozola, J.A. Influence of the preparation method in the metal-support interaction and reducibility of Ni-Mg-Al based catalysts for methane steam reforming. *Int. J. Hydrog. Energy* **2019**, *44*, 19827–19840. [[CrossRef](#)]
7. Berlier, G. Low Temperature Steam Reforming Catalysts for Enriched Methane Production. In *Enriched Methane: The First Step Towards the Hydrogen Economy*; De Falco, M., Basile, A., Eds.; Green Energy and Technology; Springer International Publishing: Cham, Switzerland, 2016; pp. 53–74. ISBN 978-3-319-22192-2.
8. Dincer, I.; Acar, C. Review and evaluation of hydrogen production methods for better sustainability. *Int. J. Hydrog. Energy* **2015**, *40*, 11094–11111. [[CrossRef](#)]
9. Yoko, A.; Fukushima, Y.; Shimizu, T.; Kikuchi, Y.; Shimizu, T.; Guzman-Urbina, A.; Ouchi, K.; Hirai, H.; Seong, G.; Tomai, T.; et al. Process assessments for low-temperature methane reforming using oxygen carrier metal oxide nanoparticles. *Chem. Eng. Process. Process Intensif.* **2019**, *142*, 107531. [[CrossRef](#)]
10. LeValley, T.L.; Richard, A.R.; Fan, M. The progress in water gas shift and steam reforming hydrogen production technologies—A review. *Int. J. Hydrog. Energy* **2014**, *39*, 16983–17000. [[CrossRef](#)]
11. Kim, H.-M.; Jang, W.-J.; Yoo, S.-Y.; Shim, J.-O.; Jeon, K.-W.; Na, H.-S.; Lee, Y.-L.; Jeon, B.-H.; Bae, J.W.; Roh, H.-S. Low temperature steam reforming of methane using metal oxide promoted Ni-Ce_{0.8}Zr_{0.2}O₂ catalysts in a compact reformer. *Int. J. Hydrog. Energy* **2018**, *43*, 262–270. [[CrossRef](#)]
12. Stefanidis, G.D.; Vlachos, D.G. High vs. low temperature reforming for hydrogen production via microtechnology. *Chem. Eng. Sci.* **2009**, *64*, 4856–4865. [[CrossRef](#)]
13. Iulianelli, A.; Liguori, S.; Wilcox, J.; Basile, A. Advances on methane steam reforming to produce hydrogen through membrane reactors technology: A review. *Catal. Rev.* **2016**, *58*, 1–35. [[CrossRef](#)]
14. Mendes, D.; Mendes, A.; Madeira, L.M.; Iulianelli, A.; Sousa, J.M.; Basile, A. The water-gas shift reaction: From conventional catalytic systems to Pd-based membrane reactors—A review. *Asia-Pac. J. Chem. Eng.* **2010**, *5*, 111–137. [[CrossRef](#)]
15. Basile, F.; Fasolini, A.; Lombardi, E. CHAPTER 7 Membrane Processes for Pure Hydrogen Production from Biomass. In *Membrane Engineering for the Treatment of Gases: Volume 2: Gas-Separation Issues Combined with Membrane Reactors (2)*; The Royal Society of Chemistry: Cambridge, UK, 2018; Volume 2, pp. 212–246. ISBN 978-1-78262-875-0.
16. Basile, F.; Fornasari, G.; Gazzano, M.; Vaccari, A. Rh, Ru and Ir catalysts obtained by HT precursors: Effect of the thermal evolution and composition on the material structure and use. *J. Mater. Chem.* **2002**, *12*, 3296–3303. [[CrossRef](#)]
17. Wang, S.; Lu, G.Q.; Millar, G.J. Carbon Dioxide Reforming of Methane to Produce Synthesis Gas over Metal-Supported Catalysts: State of the Art. *Energy Fuels* **1996**, *10*, 896–904. [[CrossRef](#)]
18. Hernandez, A.D.; Kaisalo, N.; Simell, P.; Scarsella, M. Effect of H₂S and thiophene on the steam reforming activity of nickel and rhodium catalysts in a simulated coke oven gas stream. *Appl. Catal. B Environ.* **2019**, *258*, 117977. [[CrossRef](#)]
19. Qi, A.; Wang, S.; Ni, C.; Wu, D. Autothermal reforming of gasoline on Rh-based monolithic catalysts. *Int. J. Hydrog. Energy* **2007**, *32*, 981–991. [[CrossRef](#)]
20. Wang, Y.; Chin, Y.H.; Rozmiarek, R.T.; Johnson, B.R.; Gao, Y.; Watson, J.; Tonkovich, A.Y.L.; Vander Wiel, D.P. Highly active and stable Rh/MgOAl₂O₃ catalysts for methane steam reforming. *Catal. Today* **2004**, *98*, 575–581. [[CrossRef](#)]
21. Kikuchi, E.; Tanaka, S.; Yamazaki, Y.; Morita, Y. Steam Reforming of Hydrocarbons on Noble Metal Catalysts (Part 1). *Bull. Jpn. Pet. Inst.* **1974**, *16*, 95–98. [[CrossRef](#)]
22. Martinengo, S.; Chini, P.; Giordano, G. Improved synthesis of dodecacarbonyltetrahodium at atmospheric pressure. *J. Organomet. Chem.* **1971**, *27*, 389–391. [[CrossRef](#)]
23. Ojima, I.; Donovan, R.J.; Clos, N. Rhodium and cobalt carbonyl clusters Rh₄(CO)₁₂, Co₂Rh₂(CO)₁₂, and Co₃Rh(CO)₁₂ as effective catalysts for hydrosilylation of isoprene, cyclohexanone, and cyclohexenone. *Organometallics* **1991**, *10*, 2606–2610. [[CrossRef](#)]
24. Li, C.; Widjaja, E.; Garland, M. Rh₄(CO)₁₂-catalyzed hydroformylation of cyclopentene promoted with HMn(CO)₅. Another example of Rh₄(CO)₁₂/HMn(CO)₅ bimetallic catalytic binuclear elimination. *Organometallics* **2004**, *23*, 4131–4138. [[CrossRef](#)]
25. Basini, L.; Guarinoni, A.; Aragno, A. Molecular and Temperature Aspects in Catalytic Partial Oxidation of Methane. *J. Catal.* **2000**, *190*, 284–295. [[CrossRef](#)]

26. Grunwaldt, J.-D.; Basini, L.; Clausen, B.S. In Situ EXAFS Study of Rh/Al₂O₃ Catalysts for Catalytic Partial Oxidation of Methane. *J. Catal.* **2001**, *200*, 321–329. [[CrossRef](#)]
27. Basini, L.; Marchionna, M.; Aragno, A. Drift and mass spectroscopic studies on the reactivity of rhodium clusters at the surface of polycrystalline oxides. *J. Phys. Chem.* **1992**, *96*, 9431–9441. [[CrossRef](#)]
28. Basile, F.; Mafessanti, R.; Fasolini, A.; Fornasari, G.; Lombardi, E.; Vaccari, A. Effect of synthetic method on CeZr support and catalytic activity of related Rh catalyst in the oxidative reforming reaction. *J. Eur. Ceram. Soc.* **2019**, *39*, 41–52. [[CrossRef](#)]
29. Xu, Y.; Harimoto, T.; Wang, L.; Hirano, T.; Kunieda, H.; Hara, Y.; Miyata, Y. Effect of steam and hydrogen treatments on the catalytic activity of pure Ni honeycomb for methane steam reforming. *Chem. Eng. Process. -Process Intensif.* **2018**, *129*, 63–70. [[CrossRef](#)]
30. Iglesias, I.; Baronetti, G.; Alemany, L.; Mariño, F. Insight into Ni/Ce_{1-x}Zr_xO_{2-δ} support interplay for enhanced methane steam reforming. *Int. J. Hydrog. Energy* **2019**, *44*, 3668–3680. [[CrossRef](#)]
31. Goula, M.A.; Charisiou, N.D.; Siakavelas, G.; Tzounis, L.; Tsiaoussis, I.; Panagiotopoulou, P.; Goula, G.; Yentekakis, I.V. Syngas production via the biogas dry reforming reaction over Ni supported on zirconia modified with CeO₂ or La₂O₃ catalysts. *Int. J. Hydrog. Energy* **2017**, *42*, 13724–13740. [[CrossRef](#)]
32. Tabanelli, T.; Paone, E.; Blair Vásquez, P.; Pietropaolo, R.; Cavani, F.; Mauriello, F. Transfer Hydrogenation of Methyl and Ethyl Levulinate Promoted by a ZrO₂ Catalyst: Comparison of Batch vs Continuous Gas-Flow Conditions. *ACS Sustain. Chem. Eng.* **2019**, *7*, 9937–9947. [[CrossRef](#)]
33. Chuah, G.K. An investigation into the preparation of high surface area zirconia. *Catal. Today* **1999**, *49*, 131–139. [[CrossRef](#)]
34. Chuah, G.K.; Jaenicke, S.; Cheong, S.A.; Chan, K.S. The influence of preparation conditions on the surface area of zirconia. *Appl. Catal. A Gen.* **1996**, *145*, 267–284. [[CrossRef](#)]
35. Srinivasan, R.; Harris, M.B.; Simpson, S.F.; Angelis, R.J.D.; Davis, B.H. Zirconium oxide crystal phase: The role of the pH and time to attain the final pH for precipitation of the hydrous oxide. *J. Mater. Res.* **1988**, *3*, 787–797. [[CrossRef](#)]
36. Song, W.; Popa, C.; Jansen, A.P.J.; Hensen, E.J.M. Formation of a Rhodium Surface Oxide Film in Rh_n/CeO₂(111) Relevant for Catalytic CO Oxidation: A Computational Study. *J. Phys. Chem. C* **2012**, *116*, 22904–22915. [[CrossRef](#)]
37. Velasquez, M.; Batiot-Dupeyrat, C.; Gallego, J.; Santamaria, A. Chemical and morphological characterization of multi-walled-carbon nanotubes synthesized by carbon deposition from an ethanol-glycerol blend. *Diam. Relat. Mater.* **2014**, *50*, 38–48. [[CrossRef](#)]
38. Charisiou, N.D.; Tzounis, L.; Sebastian, V.; Hinder, S.J.; Baker, M.A.; Polychronopoulou, K.; Goula, M.A. Investigating the correlation between deactivation and the carbon deposited on the surface of Ni/Al₂O₃ and Ni/La₂O₃-Al₂O₃ catalysts during the biogas reforming reaction. *Appl. Surf. Sci.* **2019**, *474*, 42–56. [[CrossRef](#)]
39. Carrero, A.; Calles, J.; Vizcaíno, A. Effect of Mg and Ca addition on coke deposition over Cu-Ni/SiO₂ catalysts for ethanol steam reforming. *Chem. Eng. J.* **2010**, *163*, 395–402. [[CrossRef](#)]
40. Galetti, A.E.; Gomez, M.F.; Arrúa, L.A.; Abello, M.C. Hydrogen production by ethanol reforming over NiZnAl catalysts: Influence of Ce addition on carbon deposition. *Appl. Catal. A Gen.* **2008**, *348*, 94–102. [[CrossRef](#)]
41. Fornasiero, P.; Kašpar, J.; Sergo, V.; Graziani, M. Redox Behavior of High-Surface-Area Rh-, Pt-, and Pd-Loaded Ce_{0.5}Zr_{0.5}O₂Mixed Oxide. *J. Catal.* **1999**, *182*, 56–69. [[CrossRef](#)]
42. Mamontov, E.; Brezny, R.; Koranne, M.; Egami, T. Nanoscale Heterogeneities and Oxygen Storage Capacity of Ce_{0.5}Zr_{0.5}O₂. *J. Phys. Chem. B* **2003**, *107*, 13007–13014. [[CrossRef](#)]
43. Lemaux, S.; Bensaddik, A.; van der Eerden, A.M.J.; Bitter, J.H.; Koningsberger, D.C. Understanding of Enhanced Oxygen Storage Capacity in Ce_{0.5}Zr_{0.5}O₂: The Presence of an Anharmonic Pair Distribution Function in the Zr–O₂ Subshell as Analyzed by XAFS Spectroscopy. *J. Phys. Chem. B* **2001**, *105*, 4810–4815. [[CrossRef](#)]
44. Luo, M.-F.; Zheng, X.-M. Redox behaviour and catalytic properties of Ce_{0.5}Zr_{0.5}O₂-supported palladium catalysts. *Appl. Catal. A Gen.* **1999**, *189*, 15–21. [[CrossRef](#)]
45. Lighthart, D.; Van Santen, R.; Hensen, E. Influence of particle size on the activity and stability in steam methane reforming of supported Rh nanoparticles. *J. Catal.* **2011**, *280*, 206–220. [[CrossRef](#)]
46. Kusakabe, K.; Sotowa, K.-I.; Eda, T.; Iwamoto, Y. Methane steam reforming over Ce–ZrO₂-supported noble metal catalysts at low temperature. *Fuel Process. Technol.* **2004**, *86*, 319–326. [[CrossRef](#)]

47. Angeli, S.D.; Turchetti, L.; Monteleone, G.; Lemonidou, A.A. Catalyst development for steam reforming of methane and model biogas at low temperature. *Appl. Catal. B Environ.* **2016**, *181*, 34–46. [[CrossRef](#)]
48. Fasolini, A.; Abate, S.; Barbera, D.; Centi, G.; Basile, F. Pure H₂ production by methane oxy-reforming over Rh-Mg-Al hydrotalcite-derived catalysts coupled with a Pd membrane. *Appl. Catal. A Gen.* **2019**, *581*, 91–102. [[CrossRef](#)]



© 2019 by the authors. Licensee MDPI, Basel, Switzerland. This article is an open access article distributed under the terms and conditions of the Creative Commons Attribution (CC BY) license (<http://creativecommons.org/licenses/by/4.0/>).